Journal of Global Positioning Systems (2023)
Vol. 19, Joint No. 1 & No. 2: 99-112
DOI:10.5081/jgps.19.1.99

Global and Regional Consistency of VTECs Inversed by IPM and GNSS

Yunri Fu[1], Ling Yang[1], Liping Fu[2,3,4], Ruyi Peng[2,3,4]

[1]College of Surveying and Geo-informatics, Tongji University, Shanghai 200092, China
[2]National Space Science Center, Chinese Academy of Sciences;
[3]Beijing Key Laboratory of Space Environment Exploration;
[4]Key Laboratory of Science and Technology on Space Environment Situational Awareness, CAS: Beijing 100190, China
Corresponding authors: Ling Yang, lingyang@tongji.edu.cn

Abstract: The ionospheric photometer (IPM) onboard the Fengyun-3D satellite is the first optical remote sensing payload in China designed for space-based surveillance of the ionosphere and capable of inversing the Vertical Total Electron Content (VTEC) at night with high sensitivity. Using the VTECs inversed by IPM, along with other sources of ionospheric observations, such as the ground-based Global Satellite Navigation System (GNSS) VTECs, ionospheric modeling can be established based on multi-source space observation techniques and is expected to improve the modeling accuracy in marine areas. Before the ionospheric modeling using multi-source data, the consistency between different sources of VTECs should be analyzed. However, the consistency between the IPM-VTEC and GNSS-VTEC has not been adequately investigated. The authors employ the Global Ionospheric Map (GIM) products from the International GNSS Service to assess the global-scale consistency between them, and the analysis reveals a generally high global-scale consistency, yet the IPM-VTEC values in specific regions are too large due to the influence of auroras and ionospheric equatorial anomalies. Subsequent investigations utilize Continuous Operational Reference System (CORS) observations in China, Europe, and the United States to analyze the regional-scale consistency between IPM-VTEC and GNSS-VTEC. The results indicate strong consistency between them in Europe. Conversely, a systematic bias is discovered in the Chinese region, while poor consistency is observed in the United States region. The mean absolute deviation between the IPM-VTEC and GNSS-VTEC in these three regions is 0.49, 0.185, and 2.62/3.53 Total Electron Content Unit, respectively, and the correlation coefficient between them is 0.67, 0.70, and -0.45/-0.61, respectively.

Keywords: ionospheric photometer; GNSS; VTEC; multi-source; consistency

1 Introduction

Since the ionosphere has great impacts on satellite navigation of the Global Satellite Navigation System (GNSS), telecommunication, and related fields, ionospheric monitoring is critically important for human life (Weng et al. 2014; Jakowski 2017). With the widely distributed International GNSS Service (IGS) and Multi GNSS Experiment (MGEX) stations worldwide, a large-scale and real-time ionospheric model can be established to monitor the

ionosphere (Hernández-Pajares et al. 1999; 2009). However, due to the limited distribution of GNSS stations in the ocean and southern hemisphere, the accuracy of the ionospheric model is significantly lower in those regions (Alizadeh et al. 2011). To improve the modeling accuracy in margin regions, the Low Earth Orbit (LEO) satellite observation data could be used for ionospheric modeling based on multi-source satellite observation techniques. Before this, given the potential inaccuracies and systematic biases inherent in different ionospheric observation data, it is important to assess the consistency of multi-source data before data fusion.

Various LEO technologies, including Doppler Orbitography and Radio Positioning Intergrated by Satellite (DORIS) systems, satellite radar altimetry systems (RA), GNSS radio occultation systems (IRO), and the Ionospheric Photometer (IPM), are available for ionosphere observing. Among these techniques, IPM is relatively new and has not been investigated comprehensively for ionospheric modeling. As a payload onboard the satellite, IPM could detect the nighttime atomic oxygen line at 135.6 nm (OI 135.6 nm), by which the nighttime Vertical Total Electron Content (VTEC) can be inversed (Chamberlain, Hunten 1988). IPM has the advantages of high sensitivity at night and worldwide coverage, making it a promising technique to investigate the ionosphere.

The only IPM payload currently in orbit in China is aboard the FengYun-3D (FY-3D) satellite. This payload was activated on November 27, 2017 and has shown exceptional performance. Fu et al. (2021) introduced its observation goal, observation principle, system composition, and observation results. For the first time, Wang et al. (2021) used this IPM payload for data inversion and analysis, which is of great significance for the development of ionospheric far-UV remote sensing detection technology in China.

With the IPM-inversed VTECs and other sources of ionosphere observation data, it is feasible to enhance the accuracy of global ionosphere modeling in maritime regions. Some scholars have studied the consistency between different sources of ionosphere observation data and the algorithm for fusing these data to establish the global ionospheric VTEC model. Todorova et al. (2007; 2008) studied global ionospheric VTEC modeling by fusing ground-based GNSS observations and RA (Jason-1) data, and estimated the constant deviation between Jason-1 and GNSS. The results show that the satellite altimetry data can improve the accuracy of the global ionospheric VTEC model in the ocean area. Dettmering et al. (2011) further studied the systematic bias between multiple different observation techniques, and the variance component estimation of different source observations. Dettmering et al. (2012; 2014) introduced the method of extracting ionospheric Total Electron Content (TEC) information using DORIS dual-frequency carrier observation data and the method of global ionospheric modeling by fusing DORIS data and other observation technology data. The results show that the corrected DORIS ionosphere is in good agreement with the IGS Global Ionospheric Map (GIM) ionosphere. The root mean square (RMS) is about 2-3 Total Electron Content Unit (TECU), and the accuracy of the global VTEC model fused with DORIS data is improved by about 12%. Although there has been some research into consistency analysis and multi-source fusing of GNSS/RA/IRO TEC data, investigations on consistency analysis between GNSS and IPM TEC data are still lacking.

This paper aims to analyze the consistency between VTECs inversed by GNSS and IPM observation data. First, the GIM products provided by Ionosphere Associate Analysis Centers (IAACs) are used to evaluate the global consistency between them. Then, the GNSS observation data of the Continuous Operational Reference System (CORS) in China, Europe, and the United States are used to inverse the VTECs in these three regions, and then three schemes are designed to evaluate the regional consistency of GNSS-VTEC and IPM-VTEC. Finally, the mean absolute deviations (MADs) and correlation coefficients are calculated to quantitatively analyze their consistency. The paper is organized as follows:

Section 2 introduces the ionospheric monitoring technologies of space-based IPM and ground-based GNSS. Afterwards, the IPM-VTEC inversed results are presented in Section 3, followed by the global and regional consistency analysis results. Finally, the concluding remarks are presented in Section 4.

2 Ionospheric monitoring technology

This section will introduce the ionospheric monitoring technologies of the space-based IPM and the ground-based GNSS. The space-based IPM onboard the FY-3D satellite could detect the nighttime OI 135.6 nm, and then the VTEC could be inversed. While the ground-based GNSS utilizes the received satellite signal propagating from satellite to receiver to extract the Slant Total Electron Content (STEC) observables and convert them to VTEC by using a mapping function.

2.1 Space-based IPM ionospheric monitoring

The relationship between the airglow intensity of the nighttime OI 135.6 nm and the VTEC can be expressed as follows (Budzien et al. 2010):

$$VTEC = K\sqrt{4\pi I_{OI135.6} H_{km}} \quad (1)$$

Where $I_{OI135.6}$ represents the OI 135.6nm airglow intensity, H_{km} is the ionospheric plasma altitude in kilometers, K is a constant related to the photochemical reaction rate coefficient, and is set as 0.717 in Budzien et al. (2010).

Eq. (1) demonstrated that there is a linear relationship between the square of VTEC and the airglow intensity of the nighttime OI 135.6 nm, indicating that by utilizing the TEC measurements and OI 135.6 nm airglow intensity, the parameter K can be determined. By employing this fitted parameter K along with the IPM measured OI 135.6 nm airglow intensity, the VTEC can be inversed.

2.2 Ground-based GNSS ionospheric monitoring

Generally, ground-based GNSS ionospheric monitoring will establish ionospheric modeling to describe the spatial variations of the ionosphere. According to the size of the modeling region, ionospheric modeling can be categorized into global and regional modeling. Global ionospheric modeling generally uses GNSS observation data from widely distributed IGS and MGEX stations worldwide. For regional ionospheric modeling, GNSS observation data from stations established densely in specific areas are used, and the polynomial model and Kriging interpolation are two common ways to model the regional ionosphere. Before the ionospheric modeling, the STEC observables should be first extracted and then converted to VTEC by using a mapping function.

Generally, the single-layer model is adopted to simplify the ionosphere model, which assumes that all free electrons are concentrated in a very thin shell at height H (Schaer 1999). The intersections of the thin shell and satellite signals from satellites to receivers are called the ionosphere piercing points (IPPs). A mapping function $F(z_r^s)$ is employed to transform the line-of-sight slant ionosphere delay to the zenith path, which can be written as (Jin et al. 2012):

$$VTEC = F(z_r^s) \cdot STEC \quad (2)$$

$$F(z_r^s) = cos\left(arcsin\left(\frac{R}{R+H} \cdot \sin(\alpha \cdot z_r^s)\right)\right) \quad (3)$$

Where z_r^s is the zenith distance, $R = 6371\ km$ and $H = 506.7 km$ are the mean radius of the earth and the height of the assumed single layer respectively; α is set as a constant and is commonly set to 0.97820.

With the spherical shell assumption, the VTEC at IPPs can be inversed and used as the input data for the ionospheric modeling. In this paper, the polynomial model and Kriging interpolation are used to model the ionosphere.

The polynomial model is consistent with the regional characteristics and commonly used in regional ionospheric modeling. The polynomial model can be expressed as (Li et al. 2005) :

$$VTEC(\beta, \lambda) = \sum_{n=0}^{N} \sum_{m=0}^{M} E_{nm} (\beta - \beta_0)^n (\lambda - \lambda_0)^m \quad (4)$$

where β_0 and λ_0 represent the latitude and longitude of the geometric center within the region, while β and λ represent the latitude and longitude

of the IPP. The variables N and M represent the maximum order and degree, respectively, of the polynomial model. E_{nm} are the unknown the regional ionospheric model parameters.

Due to that the fitting function used in the polynomial model is smooth and continuous, it cannot effectively reflect the fine variations of regional ionospheric VTEC. While the spatial interpolation method, such as Kriging, is usually more sensitive to the local ionospheric anomalies. The commonly used Kriging interpolation in ionospheric modeling assumes a model for $VTEC_{true}$ at a measurement IPP near the estimated IPP as follows: (Sparks et al. 2011):

$$VTEC_{true}(\Delta x) = a_0 + a_{east}\Delta x^T \cdot \hat{e}_{east} + a_{north}\Delta x^T \cdot \hat{e}_{north} + r(\Delta x) \quad (5)$$

where $\Delta x = x_{meas} - x_{est}$ is the Euclidean distance between the measurement IPP and estimated IPP in earth-centered, earth-fixed Cartesian coordinates. The coefficients a_0, a_{east}, a_{north} represent the planar trend of the ionosphere delay, and $r(\Delta x)$ is a scalar field of the ionosphere. The VTEC measured at x_{meas} can then be modeled as

$$VTEC_{meas}(\Delta x) = I_{true}(\Delta x) + \varepsilon \quad (6)$$

$VTEC_{meas}$ represents the measured VTEC at x_{meas}, and ε is the measurement error.

Then the $VTEC_{est}$ at x_{est} is estimated as a linear combination of $VTEC_{meas}$ near the x_{est}:

$$VTEC_{est} = \sum_{\kappa=1}^{N} w_\kappa VTEC_{meas}(\Delta x_\kappa) \quad (7)$$

where N is the number of nearby IPPs, w_κ and $VTEC_{meas}(\Delta x_\kappa)$ is the weight and VTEC value at the κ-th IPP.

3 Consistency analysis

3.1 Ionosphere photometer inversion results

The ionosphere photometer onboard the Fengyun-3D satellite was activated on November 27, 2017. After six months of testing in orbit, it was formally deployed and has shown exceptional performance. The observation data are provided by the National Satellite Meteorological Center and are open for download. With those IPM observation data, the VTEC at nighttime can be inversed. To investigate the different performances of IPM-VTEC under different geomagnetic activity, the IPM-VTEC data were selected for two days with different geomagnetic conditions: September 20, 2019, during which the geomagnetic activity was calm (Dst range from -5nT to 5nT), and October 4, 2021, during which the geomagnetic activity was relatively active (Dst range from -25nT to -8nT).

Fig. 1 and Fig. 2 show the FY-3D satellite traces and the inversed VTECs during nighttime on September 20, 2019 and October 4, 2021, with the unit of TECU. Fig. 1 demonstrates that the inverted IPM-VTECs are generally stable during the night in periods of calm geomagnetic activity, and the total electron content generally does not exceed 10 TECU within the latitude range of $-40°$ to $40°$. However, due to the influence of the auroras (Jiang et al. 2020), the inversed IPM-VTECs are abnormally large in some middle-latitude regions. Fig. 2 shows that during the active period of geomagnetic activity, the inverted IPM-VTECs are relatively active, and the equatorial ionization anomaly in low-latitude regions could be detected very well by IPM, reflecting the outstanding advantage of high sensitivity. However, the inversed IPM-VTECs in some middle-latitude regions are still influenced by auroras, resulting in abnormally large inversed IPM-VTECs.

To further illustrate where the IPM-VTEC will be significantly influenced by auroras, Fig. 3 depicts the inversed IPM-VTEC during September 21-30, 2019. This figure shows that the regions affected by auroras are predominantly located within the longitude range of 50°E to 150°E and the latitude range of 50°S to 60°S, exhibiting significantly larger IPM-VTECs than in other regions. Therefore, when using multi-source data fusion to model the ionosphere, the reduced weight should be given to IPM-VTEC in those regions.

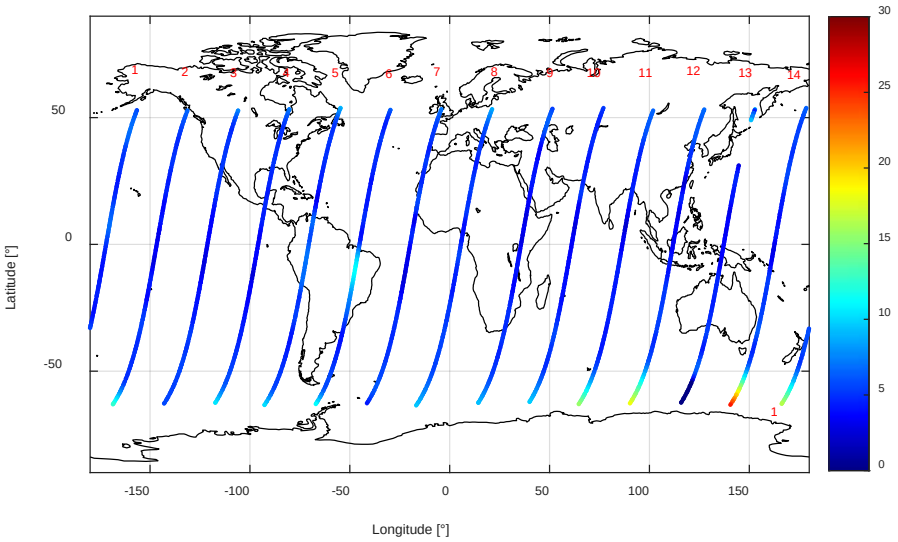

Fig. 1 IPM-VTEC inversion results on September 20, 2019.

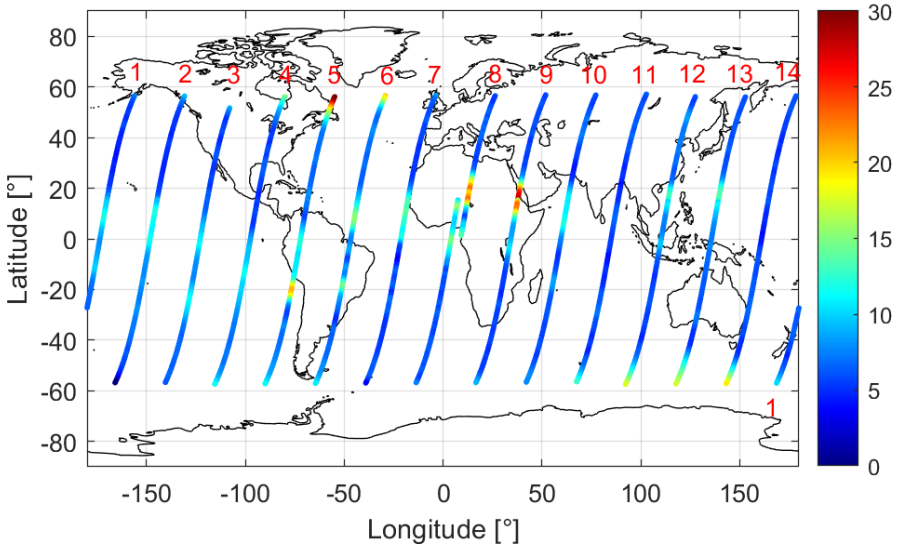

Fig. 2 IPM-VTEC inversion results on October 4, 2021.

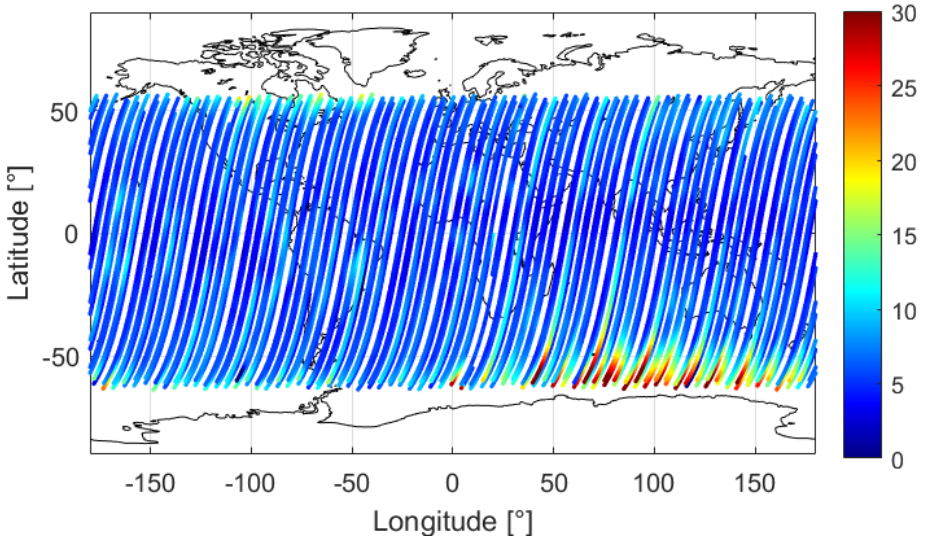

Fig. 3 IPM-VTEC inversion results during September 21-30, 2019.

3.2 Global Consistency Analysis between IPM-VTEC and GIM-VTEC

The GIM products are high-precision post-processed global grid ionospheric products provided by eight IAACs, including the Center of Orbit Determination in Europe (CODE), European Space Agency (ESA), Jet Propulsion Laboratory (JPL), Universitat Politècnica de Catalunya (UPC), Wuhan University (WHU), Chinese Academy of Science (CAS), et al. IGS's ionospheric grid products are weighted averages from these analysis centers, offering precision proven to be within 2 to 8 TECU (Hernández-Pajares et al. 2009). These high-precision ionospheric products could not only be used to improve positioning accuracy but also provide valuable data for research in fields such as atmospheric sciences, Earth dynamics, and electromagnetic physics (Hernández-Pajares et al. 1999; Roma-Dollase et al. 2018).

In this paper, the final GIM products were used to analyze the global consistency between the VTEC inversed by IPM (referred to as IPM-VTEC) and the VTEC modeled by GIM. Experimental data from September 20, 2019 and October 4, 2021 (as shown in Fig. 1 and Fig. 2) were selected, with a total of 14 bands of satellite trace for each of them. For convenience, these traces are numbered 1-14 from west to east.

Table. 1 Spatiotemporal resolution of GIM from different analysis centers

Center	CODE	ESA	IGS	JPL	UPC	WHU	CAS
Spatial Resolution	2.5° × 5°	2.5° × 5°	2.5° × 5°	2.5° × 5°	2.5° × 5°	2.5° × 5°	2.5° × 5°
Temporal Resolution	3600s	7200s	7200s	7200s	7200s	7200s	1800s

The IPM has a time sampling rate of approximately 1 second (corresponding to 0.13°), while the spatiotemporal resolutions of the GIM products of several ionospheric analysis centers are summarized in Table. 1. Due to the disparities in formats and spatiotemporal resolution between IPM and GIM, a direct analysis of their consistency is not feasible. To facilitate the assessment of consistency, two GIMs that are closest in time to an IPM sub-satellite point were initially selected. Subsequently, bilinear interpolation in space was employed to calculate the VTEC at the IPM sub-satellite point for these two GIMs. Finally, the GIM-VTEC at the specific time of the IPM sub-satellite point was determined by performing linear interpolation in time. The corresponding results for all IPM sub-satellite points shown in Fig. 1 and Fig. 2 are presented in Fig. 4 and Fig. 5, respectively. In those figures, each subplot shows the different satellite traces. The left y-axis represents the VTEC values of IPM-VTEC (the black line) and GIM-VTEC (lines with other colors) from different IAACs, while the right y-axis denotes longitude. The x-axis represents the latitude of IPM sub-satellite points. Additionally, the MADs between IPM-VTEC and GIM-TECs were also calculated and annotated in each subplot.

Fig. 4 demonstrates a relatively high consistency between IPM-VTEC and GIM-VTEC during periods of calm geomagnetic activity, particularly in the region with latitudes ranging from $-40°$ to $+40°$, where the difference between IPM-VTEC and GIM VTEC is almost only 1.5 TECU, indicating that the ionosphere was not influenced by equatorial ionization anomaly in the calm geomagnetic activity period. However, the presence of auroras has been found to exert an influence on certain traces, leading to a discernible upward trend in IPM-VTECs within the middle-latitude region (latitude above $\pm 50°$). Consequently, this phenomenon gives rise to notable deviations from IGS-VTEC. Fig. 5 also shows a relatively high consistency between IPM-VTEC and GIM-VTEC during periods of active geomagnetic activity. However, compared to Fig. 4, this consistency obviously decreases. The inversed IPM-VTEC shown in Fig. 5 is influenced not only by

auroras but also by equatorial ionization anomaly. The IPM-VTEC values in the region around latitude 20° for some traces (such as bands 8 and 9) are obviously larger than IGS-VTEC. However, apart from these regions, there is a strong agreement between IPM-VTEC and GIM-VTEC.

3.3 Regional Consistency Analysis between IPM-VTEC and CORS-VTEC

To further assess the regional consistency between IPV-VTEC and VTEC inversed from GNSS in the period of active geomagnetic activity, the IPM-VTECs on October 4, 2021, were further investigated. The observation data from CORS stations was used for inverting the GNSS VTECs. CORS serves as the GNSS infrastructure for achieving high-precision positioning and has been established by various countries worldwide. For this paper, observation data on October 4, 2021, from CORS stations in China, Europe, and the United States were selected. With these data, the STEC values can be extracted using Un-combined Precise Point Positioning (UC-PPP) method, which has been confirmed to be the most accurate method to extract the STEC observables currently available (Zhang et al. 2012; Hauschild, 2017). Then the STEC can be converted to VTEC by using a mapping function, and denoted as CORS-VTEC. The distribution of those stations and the traces of IPM sub-satellite points in the three regions are shown in Fig.6.

With those inversed CORS-VTECs, three schemes were designed to analyze the consistency between IPM-VTEC and CORS-VTEC:

Scheme 1: The regional polynomial fitting model was used to establish an ionospheric model at each epoch, and the VTECs at IPM sub-satellite points were calculated. Then, the temporal linear interpolation was conducted to match the time of IPM.

Scheme 2: The Kriging interpolation was used to interpolate the VTECs at IPM sub-satellite points, followed by temporal linear interpolation to match the time of the IPM.

Scheme 3: To mitigate the impact of model errors when employing a mathematical model to estimate the VTECs, the IPP closest to the IPM sub-satellite points in space-time was searched. This involves finding the nearest GNSS observation epoch in time for each IPM sub-satellite point and then searching for the closest IPP in space to the IPM.

Fig. 7 shows the distance (left axis) and time difference (right axis) between IPM points and their corresponding nearest IPPs for three regions. It shows that the matched IPPs are very close to IPM points in most cases, minimizing the impact of model errors as much as possible. The results for those three schemes are shown in Fig. 8, in which each subplot shows the different satellite traces. The black line in those subplots represents the IPM-VTEC, and the green, blue, and purple lines represent the results of schemes 1-3, respectively.

The upper-left panel shows the results in China. It shows that the overall trends of these three schemes are highly consistent with the IPM-VTEC. Compared to the smoothing polynomial fitting, the results of Kriging interpolation and nearest matching have higher consistency with the IPM-VTEC. Nonetheless, these results exhibit noticeable systematic biases compared to the IPM-VTEC.

The upper-right panel shows the results in Europe. The overall trends of these three schemes are also very consistent with IPM-VTEC, and there are no obviously systematic biases. However, when the latitude is below 35°, the results of polynomial fitting will deteriorate due to extrapolation. The consistency with Kriging interpolation is the highest, not only in the overall trend, but also in the local details.

The lower panel shows the results in the United States with two traces. It shows that the consistency between the IPM-VTEC and CORS-VTEC is low in this region, and both the overall trend and local variations are not similar, especially in areas with latitudes above 50°. The reason may be that the IPM-VTEC is affected by the aurora, resulting in a larger VTEC value.

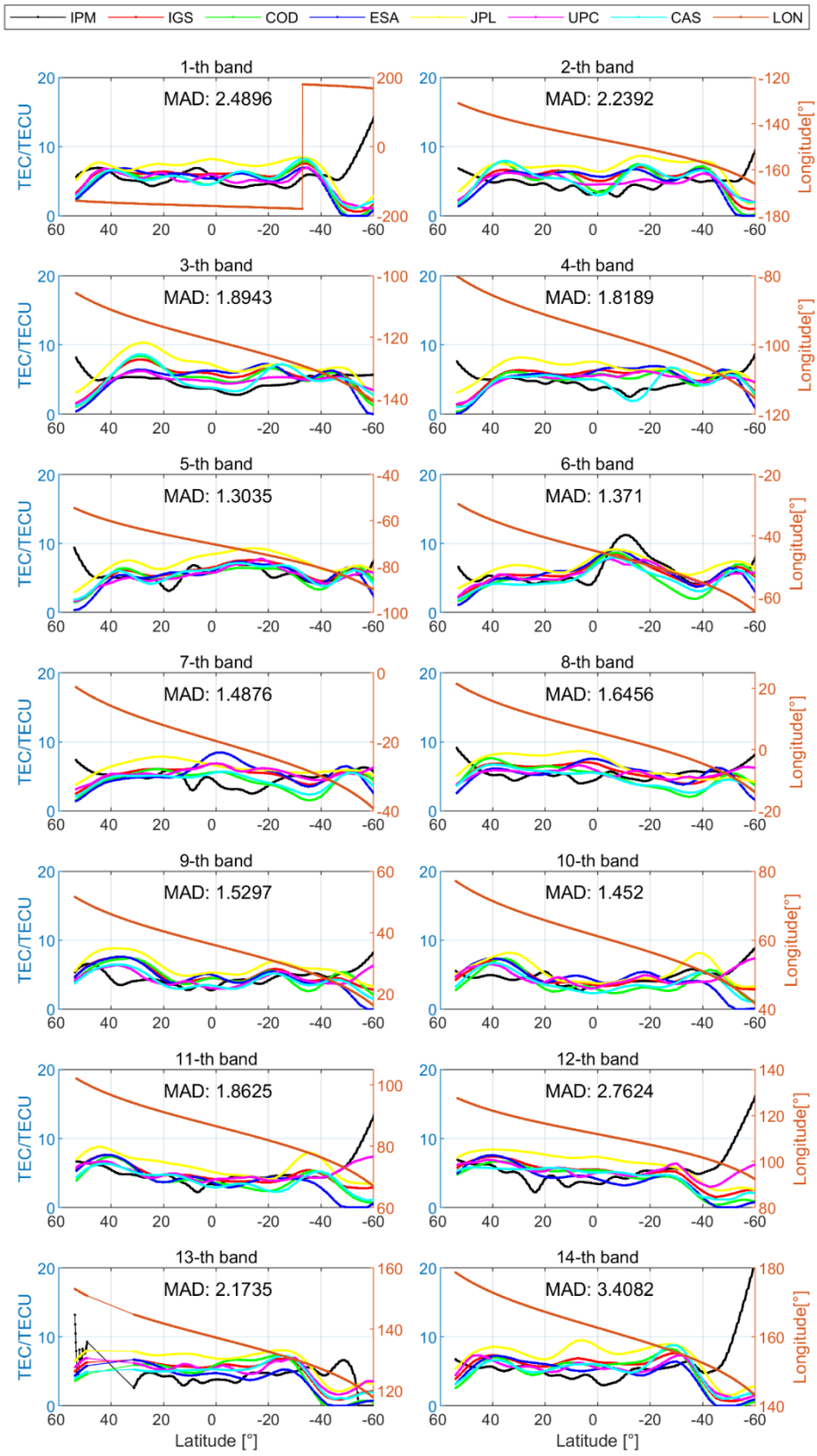

Fig. 4 The GIM-VTEC and IPM-VTEC on September 20,2019.

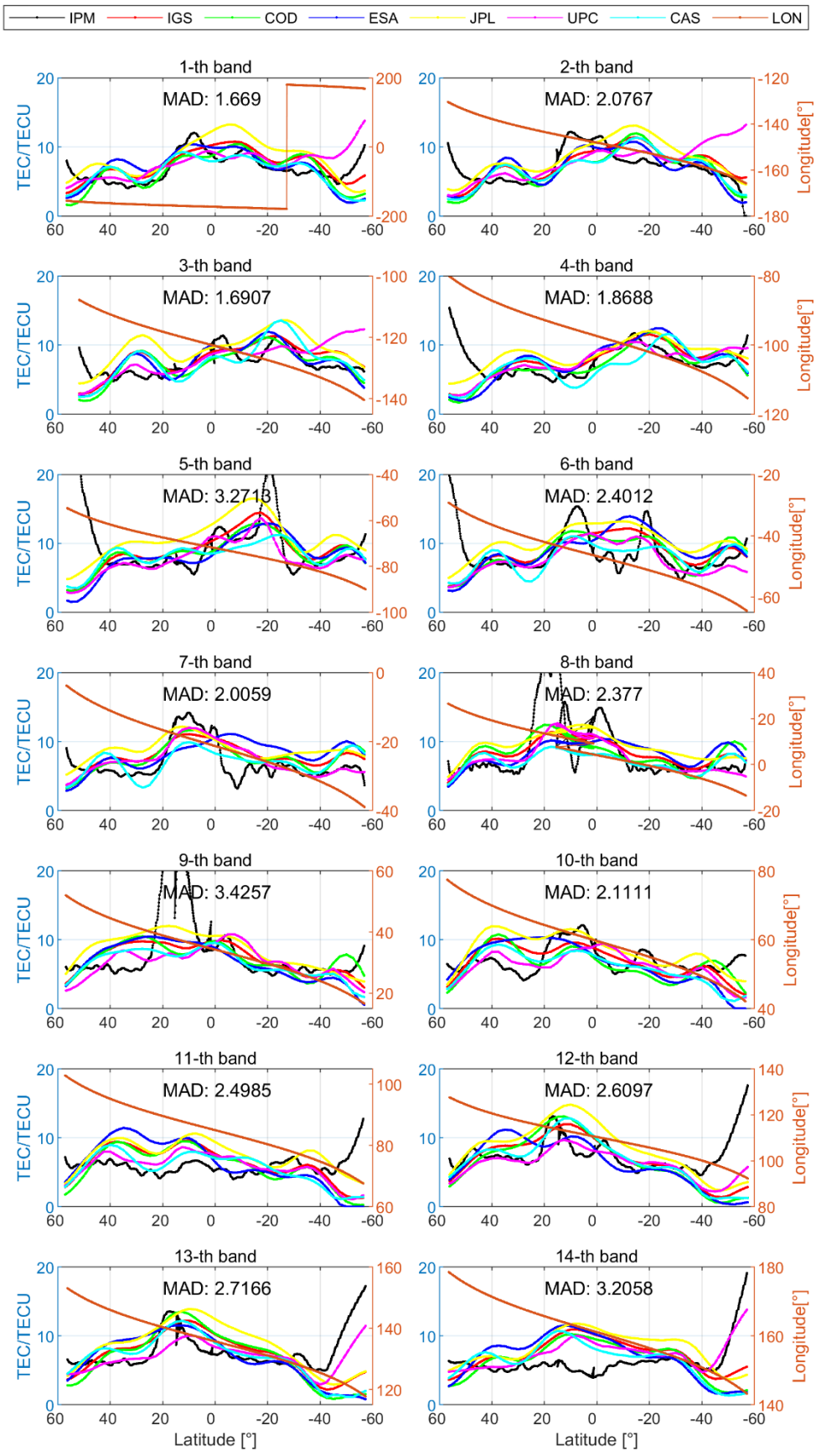

Fig. 5 The GIM-VTEC and IPM-VTEC on October 4, 2021

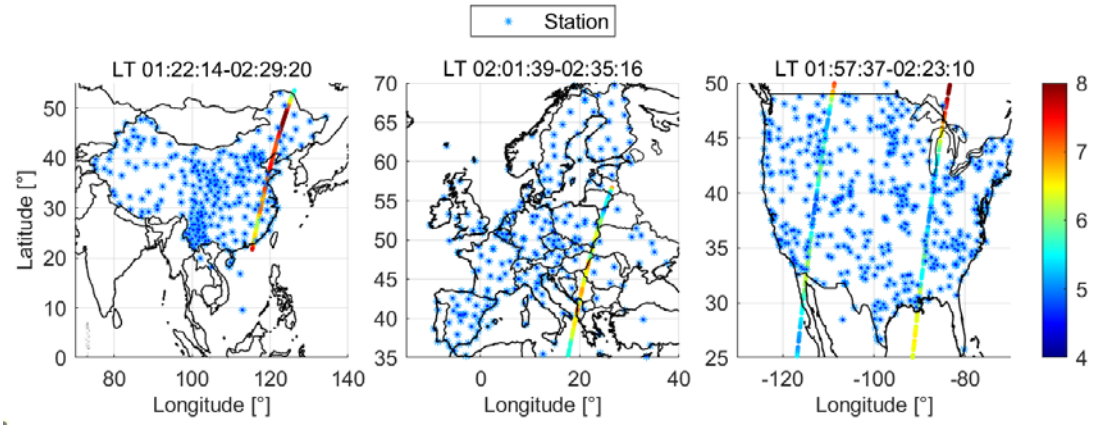

Fig.6 The distribution of CORS stations and IPM-VTEC in the regions of China, Europe, and the United States (Units: TECU).

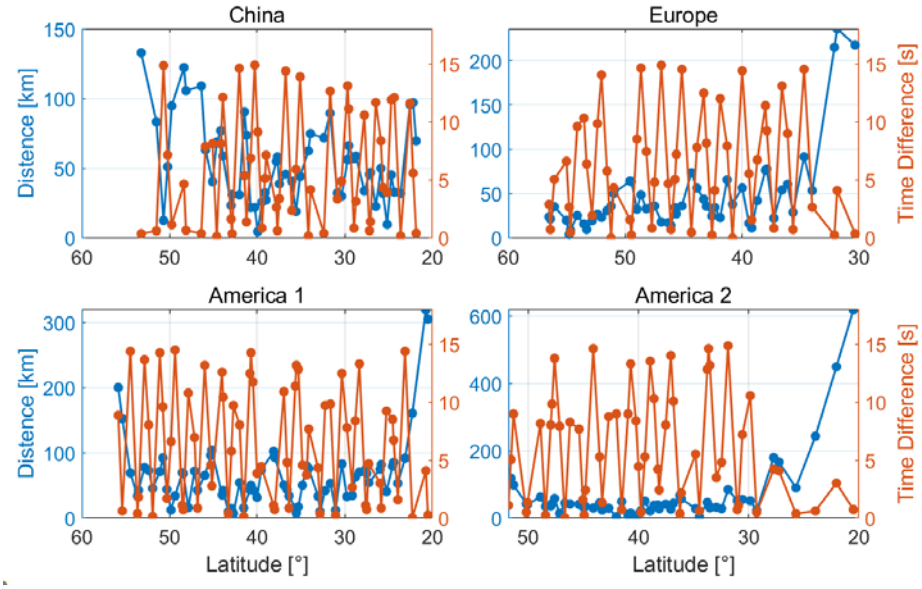

Fig. 7 Distance and time difference between IPM points and their nearest IPPs.

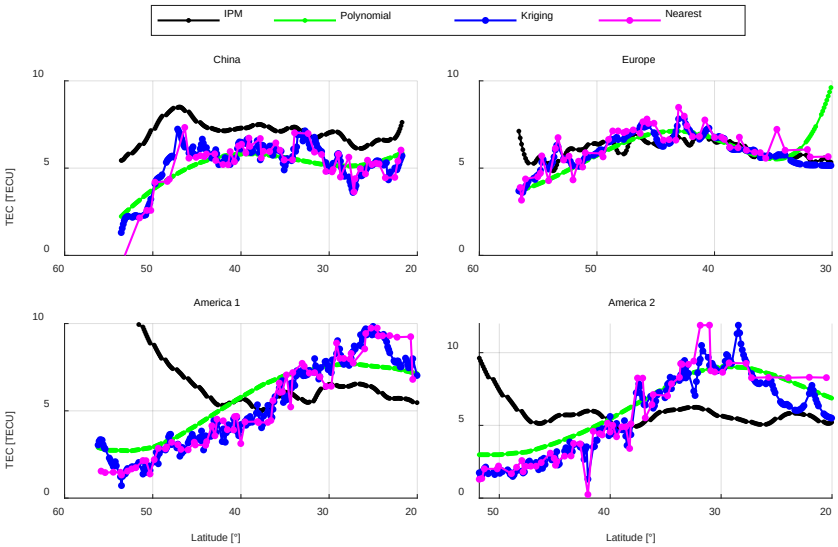

Fig. 8 Regional consistency analysis results

Since the Kriging interpolation results (referred to as Kriging-VTEC) in those three schemes could well reflect the overall trend and local variations, they were used to further quantitatively analyze the consistency between IPM-VTEC and CORS-VTEC. In this quantitative analysis, the MADs between them were calculated to assess their system deviation, and correlation coefficients were calculated to assess their trend consistency.

Before calculating the correlation coefficient, to avoid the influence of noise, the Empirical Mode Decomposition (EMD) was used to extract the trend terms of IPM-VTEC and Kriging-VTEC. EMD decomposes the original data from high frequency to low frequency into Intrinsic Mode Functions components. To extract the trend term of the data, components with amplitudes less than 1 TECU are removed, and the remaining components are added together as the trend term. Then the correlation coefficients between the two were calculated to evaluate their trend consistency. It should be noted that even the threshold of 1TECU used in this paper could effectively extract the trend term in our experiments, a varied threshold should be used under different solar activities to extract the trend term more accurately.

Fig. 9 shows the experiment results. In this figure, the black and blue dotted lines represent the IPM-VTEC and Kriging-VTEC, while the red and green solid lines represent their trend terms. This figure shows that the consistency between IPM-VTEC and Kriging-VTEC in Europe is the highest, with a correlation coefficient of 0.7 and a MAD of 0.49 TECU, indicating a relatively small systematic deviation and high trend consistency between the two. The trend consistency between Kriging-VTEC and IPM-VTEC in China is the highest, with a correlation coefficient of 0.7, but a MAD of 1.85 TECU, indicating an obvious bias, which may be attributed to the inaccurate code biases of receivers during the extraction of STEC observations. The consistency in the United States is the worst, with the opposite trend and a significant systematic deviation. The reason may be, as mentioned earlier, the influence of the aurora, resulting in a larger value of IPM-VTEC.

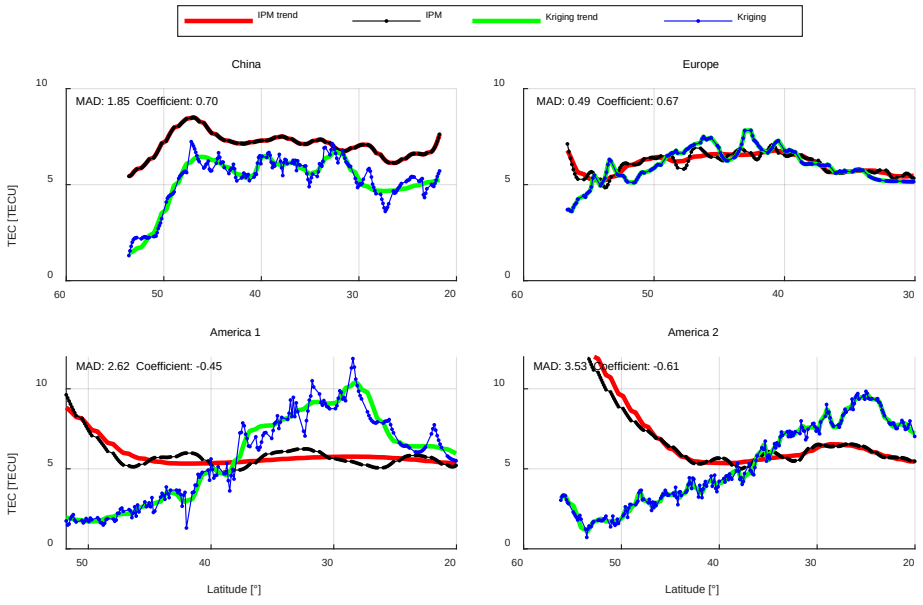

Fig. 9 The MAD and correlation coefficient between IPM-VTEC and Kriging-VTEC

4 Concluding remarks

The ionospheric photometer onboard the Fengyun-3 D satellite has the advantage of high sensitivity at night and could achieve all-weather monitoring of key ionospheric information. This paper first utilizes GIM products to analyze the consistency of GIM-VTEC and IPM-VTEC on a

global scale. The results indicate that the overall consistency between the two is high, but due to the influence of aurora and ionospheric equatorial anomalies, the IPM-VTEC values in certain regions are abnormally higher. Subsequently, observations of CORS stations are used to inverse the VTEC, and three schemes were designed to validate the effectiveness of IPM-VTEC in the regions of China, Europe, and the United States. The experimental results show that in the European region, the consistency between the IPM-VTEC and CORS-VTEC is highest, and there is no significant systematic bias; in the Chinese regions, there is a systematic bias between the IPM-VTEC and CORS-VTEC; and in the United States region, the consistency between the two is poor.

In the future, new evaluation indicators will be introduced to characterize the consistency of the IPM and GNSS inversion results, and a comprehensive analysis of the data over the past five years will be conducted to clarify the reasons for the differences in the IPM and GNSS inversion results. Finally, the optimal fusion of the two will be studied to compensate for the insufficient ionospheric data in marine areas.

Reference

Alizadeh MM, Schuh H, Todorova S, Schmidt M (2011) Global Ionosphere Maps of VTEC from GNSS, satellite altimetry, and Formosat-3/COSMIC data. J Geod 85(12), 975-987. https://doi.org/10.1007/s00190-011-0449-z

Budzien SA, Chua DH, Coker C, et al. (2010) Evolved Tiny Ionospheric Photometer (ETIP): a sensor for ionospheric specification. In: 2010 Decadal Strategy for Solar and Space Physics. Washington DC: National Academies Press.

Chamberlain TP, Hunten DM (1988) Theory of Planetary Atmospheres: An Introduction to Their Physics and Chemistry. Academic Press.

Dettmering D, Heinkelmann R, Schmidt M (2011) Systematic differences between VTEC obtained by different space-geodetic techniques during CONT08. J Geod 85, 443-451. https://doi.org/10.1007/s00190-011-0473-z

Dettmering D, Schmidt M, Limberger M. (2012). Contributions of DORIS to ionosphere modeling. IDS workshop, Venice, Italy.

Dettmering D, Limberger M, Schmidt M (2014) Using DORIS measurements for modeling the vertical total electron content of the Earth's ionosphere.J Geod 88(12), 1131-1143. https://doi.org/10.1007/s00190-014-0748-2

Fu LP, Peng RY (2021) The ionosphere photometer (IPM) onboard China's meteorological satellite FY-3D. Spacecr. Environ. Eng. 38(3), 305-310. https://doi.org/10.12126/see.2021.03.010

Jakowski N (2017) Ionosphere Monitoring. In: Teunissen PJG, Montenbruck O (Eds.) Springer Handbook of Global Navigation Satellite Systems. Springer International Publishing, Cham, pp. 1139-1162. https://doi.org/10.1007/978-3-319-42928-1_39

Jiang F, Mao T, Li XY, et al. (2014) The research on NmF2 and TEC derived from nighttime OI 135.6 nm emission measurement. Chin. J. Geophys. 57(11), 3679-3687.

Jiang F, Mao T, Zhang XX, et al. (2020). Observation of thermosphere and ionosphere using the ionosphere photometer (IPM) on the Chinese meteorological satellite FY-3D. Adv. Space Res. 66(9), 2151-2167. https://doi.org/10.1016/j.asr.2020.07.027

Jin R, Jin S, Feng G (2012) M_DCB: Matlab code for estimating GNSS satellite and receiver differential code biases. GPS Solut. 16: 541-548. https://doi.org/10.1007/s10291-012-0279-3

Hernandez-Pajares M, Juan JM, Sanz J (1999) New approaches in global ionospheric determination using ground GPS data. J Atmos Sol-Terr Phy 61(16):1237–1247.https://doi.org/10.1016/S1364-6826(99)00054-1

Hernández-Pajares M, Juan JM, Sanz J, et al. (2009) The IGS VTEC maps: a reliable source of ionospheric information since 1998. J Geod 83:

263-275. https://doi.org/10.1007/s00190-008-0266-1

Hauschild A (2017) Basic Observation Equations. In: Teunissen PJG, Montenbruck O (Eds.) Springer Handbook of Global Navigation Satellite Systems. Springer International Publishing, Cham, pp. 561-582. https://doi.org/10.1007/978-3-319-42928-1_19

Li ZH, Huang JS. (2005). Error Sources in GPS Positioning. In: GPS Surveying and Data Processing. Wuhan University Press, Wuhan, pp. 38–77.

Roma-Dollase D, Hernández-Pajares M, et al. (2018) Consistency of seven different GNSS global ionospheric mapping techniques during one solar cycle. J Geod 92, 691-706. https://doi.org/10.1007/s00190-017-1088-9

Schaer S (1999) Mapping and predicting the earth's ionosphere using the global positioning system. Dissertation, University of Bern

Sparks L, Blanch J, Pandya N (2011a) Estimating ionospheric delay using kriging: 1. Methodology. Radio Sci. 46(06): 1-13. https://doi.org/10.1029/2011RS004667

Todorova S, Schuh H, Hobiger T, Hernandez-Pajares M. (2007). Impact of the Combination of GNSS and Altimetry Data on the Derived Global Ionosphere Maps. In: American Geophysical Union, Acapulco, Mexico.

Todorova S, Hobiger T, Schuh H. (2008). Using the Global Navigation Satellite System and satellite altimetry for combined Global Ionosphere Maps. Adv. Space Res. 42, 727-736.

Wang DX, Fu LP, Jiang F, Jia N, Wang TF, Dou ST (2021) Inversion of Ionospheric O/N2 by Using FY-3D Ionospheric Photometer Data. Spectrosc. Spect. Anal. 41(4), 1004-1010. http://www.gpxygpfx.com/CN/10.3964/j.issn.1000-0593(2021)04-1004-07

Weng DJ, Ji SY, Chen W, Liu ZZ (2014) Assessment and Mitigation of Ionospheric Disturbance Effects on GPS Accuracy and Integrity. J Navig 67(3), 371–384. https://doi.org/10.1017/S0373463314000046

Zhang B, Ou J, Yuan Y, Li Z. (2012). Extraction of line-of-sight ionospheric observables from GPS data using precise point positioning. Sci. China Earth Sci. 55(11), 1919–1928. https://doi.org/10.1007/s11430-012-4454-8.

Authors

Yunri Fu received the B.S. degree in survey engineering from Henan Polytechnic University, Henan, China, in 2020. He is currently pursuing the Ph.D. degree in the College of Surveying and Geo-informatics, Tongji University. His research interests include the atmosphere delay modeling and integrity monitoring.

Ling Yang received the B.S. and M.S. degrees in survey engineering from Tongji University, Shanghai, China, and received a Ph.D. degree in surveying and spatial information from the University of New South Wales (UNSW), Sydney, Australia, in2014. She is currently an Associate Professor at the College of Surveying and Geoinformatics, Tongji University. Her research interests include quality control for GNSS+ positioning and navigation.

Liping Fu received the Ph.D degree in Wuhan Institute of Physics and Mathematics, CAS, Hubei, China, in 1999. She is a professor in National Space Science Center, Chinese Academy of Science. Her research interests

include the optical remote sensing technique and data analysis in space weather.

Ruyi Peng received his B.S. degree from Southwest Minzu University in 2011 and Ph.D. degree at University of Chinese Academy of Sciences in 2016. He joined the National Space Science Center of the Chinese Academy of Sciences after graduation and became a senior engineer in 2019. His current research interests are in the ultraviolet-based science and detection technique in the lunar and planetary exploration.